Appl. Phys. B 86, 537–545 (2007)
DOI: 10.1007/s00340-006-2439-z

Applied Physics B
Lasers and Optics

T. SUSDORF[1]
D. DEL AGUA[1,*]
A. TYAGI[1]
A. PENZKOFER[1,✉]
O. GARCÍA[2]
R. SASTRE[2]
A. COSTELA[3]
I. GARCÍA-MORENO[3]

Photophysical characterization of pyrromethene 597 laser dye in silicon-containing organic matrices

[1] Institut II – Experimentelle und Angewandte Physik, Universität Regensburg, Universitätsstrasse 31, 93053 Regensburg, Germany
[2] Instituto de Ciencia y Tecnología de Polímeros, CSIC, Juan de la Cierva 3, 28006 Madrid, Spain
[3] Instituto de Química Física "Rocasolano", CSIC, Serrano 119, 28006 Madrid, Spain

Received: 30 June 2006
Published online: 9 September 2006 •

ABSTRACT Samples of dipyrromethene-BF_2 dye PM597 incorporated in copolymers of 3-(trimethoxysilyl)propyl methacrylate (TMSPMA) with methyl methacrylate (MMA) and 2-hydroxyethyl methacrylate (HEMA), and in terpolymers of MMA, HEMA and TMSPMA are characterized. The absorption cross-section spectra, stimulated emission cross-section spectra, and the excited-state absorption cross-section at 527 nm are determined. The fluorescence quantum distributions and fluorescence lifetimes are measured. The photo-degradation is studied under cw laser excitation conditions and quantum yields of photo-degradation are extracted. PM597 solid state samples are compared with PM597 in liquid ethyl acetate solution. The fluorescence quantum yield of PM597 is higher in doped samples (around 70%) compared to PM597 in ethyl acetate (43%). The excited-state absorption cross-section was found to be negligibly small. The photo-stability is considerably larger in the polymeric samples compared to the liquid solutions.

PACS 42.55.-f; 78.45.+h; 78.55.-m; 78.40.Me

1 Introduction

The development of tunable solid-state organic dye lasers is a subject of considerable interest and research activity [1]. Compared to conventional liquid dye lasers they have the advantage of being free of solvent handling, having a small size, and being easy to operate. For high-performance solid-state dye lasers highly photo-stable dyes with low quantum yield of triplet formation and low triplet absorption cross-section in the lasing wavelength region are required.

The dipyrromethene dyes are well established laser dyes with low triplet absorption losses in the laser emission region [2]. They find application in solid-state dye lasers because of their high laser efficiency and high photo-stability [1, 3, 4]. The dye pyrromethene 567 (PM567) has been applied in solid-state lasers [5–11]. It is tunable over a wavelength range from 545 nm to 585 nm [8]. At the 8-position modified dyes of PM567 were synthesized, doped into polymer matrices and covalently bound to polymers in order to improve their laser performance and photo-stability [4, 10–15].

The dye pyrromethethene 597 (PM597, full name: 1,3,5,7,8-pentamethyl-2,6-di-t-butylpyrromethene-difluoroborate complex) was used as gain medium in various solid-state lasers with high performance data [8, 16–24]. Laser wavelength tuning was achieved over a range from 572 nm to 612 nm in the solid state lasers [8]. Amplified spontaneous emission and phase-conjugated backward stimulated emission was achieved on PM597 in PMMA [25]. The laser performance degradation with the number of shots of PM597 solid-state dye lasers was studied in [19, 20, 22]. The photophysical properties of PM597 in organic solvents was studied in detail in [26]. The photo-degradation of PM597 in acetonitrile and n-hexane was analyzed in [27].

In this paper some photo-physical characterization (absorption and emission spectra, fluorescence quantum yields and lifetimes, excited-state absorption, and photo-degradation) of the dye PM597 in silicon-containing organic matrices [22] is carried out. These matrices are (i) copolymers of methyl methacrylate (MMA) with 3-(trimethoxysilyl)propyl methacrylate (TMSPMA) called COP(MMA-TMSPMA), (ii) sol–gel hydrolysis condensed copolymers of MMA with TMSPMA called COPH(MMA-TMSPMA), (iii) copolymers of 2-hydroxyethyl methacrylate (HEMA) and TMSPMA called COP(HEMA-TMSPMA), and (iv) terpolymers of MMA, HEMA and TMSPMA called TERP(MMA-HEMA-TMSPMA). The behaviour of PM597 in these polymer matrices is compared with the behaviour of PM597 in the solvent ethyl acetate. The structural formulae of PM597, MMA, HEMA, and TMSPMA are shown in Fig. 1.

2 Experimental

The dipyrromethene-BF_2 dye PM597 used in the dye doped polymer preparation was purchased from Exciton, and used as received. For spectroscopy studies on PM597 in ethyl acetate, PM597 was bought from Radiant Dyes. The other used chemicals, MMA, HEMA, TMSPMA, and 2, 2′-azobis(isobutyronitrile) (AIBN) were purchased from Aldrich. MMA, HEMA, and TMSPMA were vacuum distilled. AIBN was re-crystallized in ethanol before use. This is

✉ Fax: +49-941-9432754,
E-mail: alfons.penzkofer@physik.uni-regensburg.de
*On leave from Instituto de Ciencia y Tecnología de Polímeros, CSIC, Juan de la Cierva 3, 28006 Madrid, Spain

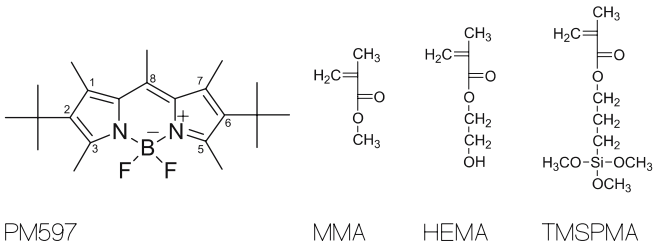

FIGURE 1 Structural formulae of dipyrromethene-BF_2 dye PM597 (sum formula: $C_{22}H_{33}BF_2N_2$, molar mass: $M = 374.32\,\mathrm{g\,mol^{-1}}$), methyl methacrylate (MMA, $C_5H_8O_2$, $M = 374.32\,\mathrm{g\,mol^{-1}}$, density $\varrho = 0.936\,\mathrm{g\,cm^{-3}}$), 2-hydroxyethyl methacrylate (HEMA, $C_6H_{10}O_3$, $M = 130.14\,\mathrm{g\,mol^{-1}}$, $\varrho = 1.074\,\mathrm{g\,cm^{-3}}$), and 3-(trimethoxysilyl)propyl methacrylate (TMSPMA, $M = 422.81\,\mathrm{g\,mol^{-1}}$, $\varrho = 0.918\,\mathrm{g\,cm^{-3}}$)

the thermal polymerization initiator of choice, since it leaves UV-transparent end groups on the copolymer.

All copolymers and terpolymers are obtained by radical bulk polymerization using AIBN of appropriate concentration (0.5 wt. %) with regard to the total amount of organic monomers in the polymerization mixture. An adequate amount of PM597 dye was added to freshly purified TMSPMA and the mixture was ultrasonically irradiated until complete dissolution of the dye was achieved. Mixtures with different volume/volume proportions of monomers were prepared. The resulting solutions were filtered through 2 μm pore size filters (Whatman Lab, PTFE disposable filters) into appropriate cylindrical polypropylene moulds. The polymerization was performed in a thermal bath kept at 40 °C for two days. The temperature was then raised to 45 °C and kept there for about one day. Following this the temperature was increased to 50 °C and kept there for one day. After that the temperature was raised up to 80 °C over a time period of one day in order to decompose any residual AIBN. Finally, the temperature was decreased in steps of 5 °C per day, down to room temperature, and after that the samples were un-moulded. The described procedure reduced stress in the polymer samples due to thermal shock.

The synthesis of COPH(MMA-TMSPMA) was based on "in situ" and simultaneous hydrolysis-condensation of methoxy groups of TMSPMA during the free radical bulk polymerization of MMA using AIBN. The sol–gel process of the alkoxide TMSPMA was catalyzed by adding, under stirring, a mixture of water and hydrochloric acid (HCl). The mole ratios $[\mathrm{HCl}]/[\mathrm{TMSPMA}] = 1.85 \times 10^{-2}$ and $[\mathrm{H_2O}]/[\mathrm{TMSPMA}] = 1.5$ were adjusted. The appropriate amount of PM597 was dissolved in the MMA to achieve a concentration of approximately $9 \times 10^{-6}\,\mathrm{mol\,dm^{-3}}$ in the final MMA-TMSPMA solutions. The solutions were treated ultrasonically to ensure the molecular PM597 dissolution. Since pyrromethene dyes lose their lasing ability under acid or basic conditions [28], pyridine was added to the TMSPMA-HCl-H_2O solutions in order to decrease the H^+ concentration to pH > 6, before the addition of PM597 in MMA. The resulting mixture was poured into cylindrical moulds of polypropylene (≈ 14 mm diameter) for the purpose of obtaining a geometric configuration close to that required for the solid-state dye laser samples. The moulds were kept in an oven at 45–50 °C for 1–2 months. The temperature was then increased linearly to 80 °C within one week. After that the temperature was reduced to room temperature in steps of 5 °C per day. At room temperature the samples were un-moulded. Cylindrical monoliths of 3–4 $\mathrm{cm^3}$ were obtained with good mechanical properties [29].

The refractive index spectra of the samples have been determined by total internal reflection measurement with an Abbe refractometer (Zeiss, model B) using white-light illumination and Amici prism dispersion compensation. The method allows the determination of the refractive index n_D at wavelength $\lambda_\mathrm{D} = 589.3$ nm and the dispersion value $n_\mathrm{F} - n_\mathrm{C}$, where n_F is the refractive index at $\lambda_\mathrm{F} = 486.1$ nm and n_C is the refractive index at $\lambda_\mathrm{C} = 656.3$ nm [30]. From n_D and $n_\mathrm{F} - n_\mathrm{C}$ the refractive index dispersion was determined approximately by using a single oscillator model with the relation [31]

$$\frac{n^2(\lambda)-1}{n^2(\lambda)+2} = \frac{\kappa}{1/\lambda_0^2 - 1/\lambda^2}\,, \tag{1}$$

where the unknowns, κ and λ_0, are calculated numerically from the known values $n(589.3\,\mathrm{nm})$ and $n(486.1\,\mathrm{nm}) - n(656.3\,\mathrm{nm})$. Solving of (1) to n gives

$$n = \left(\frac{1/\lambda_0^2 - 1/\lambda^2 + \kappa}{1/\lambda_0^2 - 1/\lambda^2 - \kappa}\right)\,. \tag{2}$$

The absorption cross-section spectra are extracted from transmission measurements. The PM597 doped samples and the blanks of equal polymer composition and thickness were measured. The absorption coefficient spectra are given by $\alpha(\lambda) = -\ln(T_\mathrm{s}/T_\mathrm{b})/\ell$, where T_s is the transmission of the dye doped sample, T_b is the transmission of the corresponding blank, and ℓ is the sample length. The absorption cross-section is related to the absorption coefficient by $\sigma(\lambda) = \alpha(\lambda)/N_0$, where N_0 is the number density of PM597 molecules ($N_0 = CN_\mathrm{A}/1000$, where C is the concentration in $\mathrm{mol\,dm^{-3}}$, N_A is the Avogadro constant, and N_0 is the number density in $\mathrm{cm^{-3}}$). Since the number density of dye molecules in the polymer samples is not exactly known, the absorption cross-section spectra of the polymer samples are normalized to the absorption cross-section spectrum, $\sigma_\mathrm{a,EtAc}(\lambda)$, of PM597 in ethyl acetate according to $\sigma_\mathrm{a}(\nu) = \alpha(\nu)[\int_{S_0-S_1}\sigma_\mathrm{a,EtAc}(\nu)\,\mathrm{d}\nu / \int_{S_0-S_1}\alpha(\nu)\,\mathrm{d}\nu]$, where $S_0 - S_1$ indicates the range of integration over the $S_0 - S_1$ absorption region.

The fluorescence quantum distribution, $E_\mathrm{F}(\lambda)$, and fluorescence quantum yield, φ_F, measurements were carried out with a self-assembled fluorimeter in front-face fluorescence signal collection arrangement [32, 33] (excitation wavelength 500 nm). Rhodamine 6G in methanol was used as the reference dye ($\varphi_\mathrm{F,R} = 0.94$ [34]). The degree of fluorescence polarisation [35] $P_\mathrm{F} = (S_{\mathrm{F},||} - S_{\mathrm{F},\perp})/(S_{\mathrm{F},||} + S_{\mathrm{F},\perp})$ was determined by vertical polarized fluorescence excitation combined with vertical polarized ($S_{\mathrm{F},||}$) and horizontal polarized ($S_{\mathrm{F},\perp}$) fluorescence signal detection.

The fluorescence lifetimes, τ_F, were measured by picosecond pulse excitation with second harmonic pulses of a mode-locked Ti:sapphire laser (femtosecond laser system Hurricane from Spectra-Physics, excitation wavelength 400 nm, pulse duration ≈ 3 ps) and fluorescence signal registration with a fast micro-channel-plate photomultiplier (Hamamatsu type

R1564-U01) and a high-speed digital oscilloscope (LeCroy type DSO 9362).

The saturable absorption of some samples at 527 nm was studied by intensity dependent transmission measurement [36] with second harmonic pulses of a mode-locked Nd:glass laser (wavelength $\lambda_L = 527$ nm, pulse duration $\Delta t_L = 6$ ps) [37].

The photo-stability of the samples was studied by cw Ar-ion laser excitation at $\lambda_L = 514$ nm (excitation to first excited singlet state). The PM597 doped polymer samples were excited through an aperture of 2 mm in diameter. The liquid samples of PM597 in ethyl acetate were exposed in a small-volume cell of 1.5 mm thickness, 1.5 mm width and 5 mm height. The transmission of the excitation laser light was measured with two silicon photodetectors. Absorption spectra and fluorescence spectra were taken after certain durations of exposure. The quantum yield of photo-degradation, φ_D, is determined by the ratio of the number of degraded molecules, ΔN_D, to the number of absorbed photons, $\Delta n_{ph,abs}$, i.e.

$$\varphi_D = \frac{\Delta N_D}{\Delta n_{ph,abs}} . \tag{3}$$

After a certain exposure time, t_1 (exposed energy density, $w_L(t_1) = I_L t_1$), the number density of degraded molecules in a time interval, $\delta t = t_2 - t_1$, is given by

$$\Delta N_D = \frac{-\{\ln[T(t_1, \lambda_{pr})] - \ln[T(t_2, \lambda_{pr})]\}}{\sigma_a(\lambda_{pr})} = \ln(10)\frac{A(t_1, \lambda_{pr}) - A(t_2, \lambda_{pr})}{\sigma_a(\lambda_{pr})} , \tag{4}$$

and the number density of absorbed photons is

$$\Delta n_{ph,abs} = \frac{w_L(t_2) - w_L(t_1)}{h\nu_L}\left[1 - \frac{T(t_1, \lambda_L) + T(t_2, \lambda_L)}{2}\right] . \tag{5}$$

In (3) the absorbance, A, is defined by $A = -\log(T) = -\ln(T)/\ln(10)$.

3 Results

The transmission spectra of the polymeric blanks (un-doped samples) are shown in Fig. 2 for the different classes and compositions. The polymer composition is given in volume ratios. All samples had a length of 1.1 cm and a diameter of 1.1 cm. They were measured against air. The transmissions, T_R, due to light reflection, R, are included. They are calculated by the relations, $T_R = (1-R)/(1+R)$, and $R = (n-1)^2/(n+1)^2$, where n is the refractive index. The transmission of ethyl acetate in a 1 cm cell versus a 1 cm water-filled reference cell is included in Fig. 2a. For the polymer blanks the transmission reduction starts already in the 700 nm to 600 nm region, and the transparency range ends at about 300 nm (transmission becomes less than 5% in the samples of 1.1 cm length). A blank COPH(MMA-TMSPMA) sample was not available. The transmission edge of ethyl acetate is at about 250 nm. For each class of blanks the $S_0 - S_1$ transmission spectrum of a 1 cm long dye doped sample is included. For blank COP(MMA-TMSPMA) the long-wavelength transmission is lower than

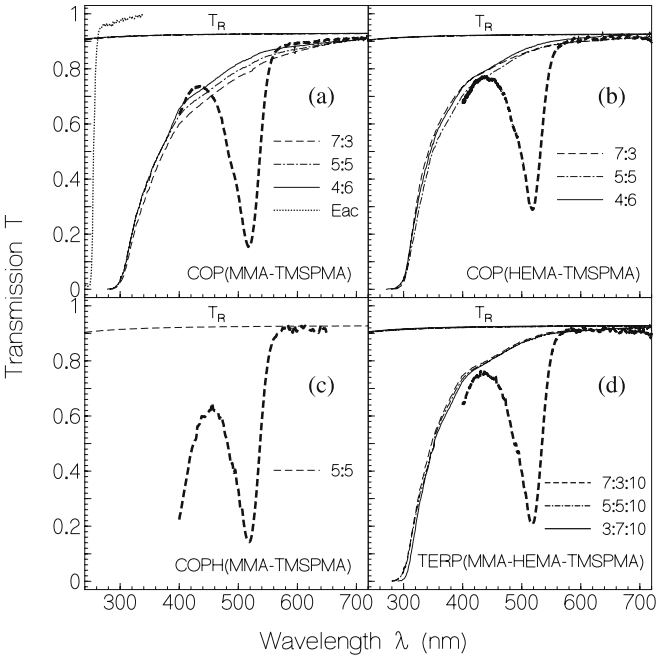

FIGURE 2 Transmission spectra of blank polymer substrates and of PM597 doped samples. Sample thickness 11 mm. The PM597 concentration is given in Table 1. In (**a**) the neat transmission of ethyl acetate in a 1 cm cell is included (*dotted curve*).

in the PM597 doped samples (see Fig. 2a). This may indicate better homogenous polymerisation in the presence of PM597.

In Fig. 3 the refractive index spectra of polymer blanks, determined as explained above, are shown. For COPH(MMA-TMSPMA) the dye doped sample was measured. For the four different polymer classes the absolute refractive indices and

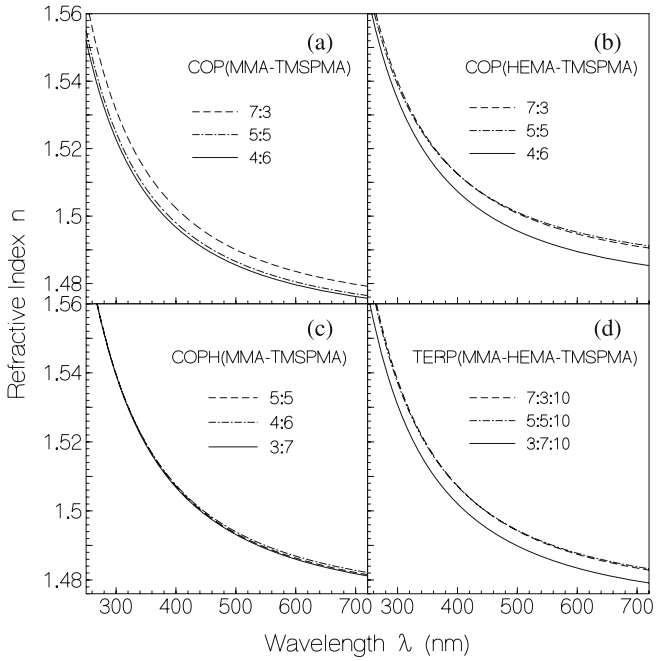

FIGURE 3 Refractive index spectra of blank polymer samples

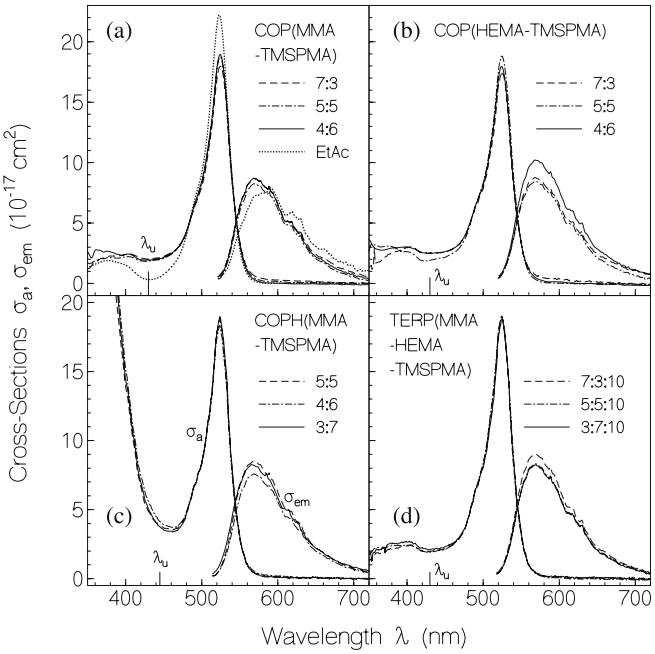

FIGURE 4 Absorption cross-section spectra of PM597 doped polymer samples

the refractive index dispersion are nearly the same with values in the range of 1.48 to 1.50 at 530 nm.

The absorption cross-section spectra of the investigated samples are shown in Fig. 4. They are extracted from the transmission measurements and normalized to the same $S_0 - S_1$ absorption cross-section integral as measured for PM597 in ethyl acetate. The absorption cross-section spectrum of PM597 in ethyl acetate is included in Fig. 4a (dotted curve). For all samples the absorption peak is at $\lambda_{a,p} = 524 \pm 1$ nm. The spectral half-width (FWHM) of the $S_0 - S_1$ absorption band is slightly narrower in ethyl acetate ($\Delta\tilde{\nu}_a \approx 1150\,\mathrm{cm}^{-1}$) than in the polymer matrices ($\Delta\tilde{\nu}_a \approx 1300\,\mathrm{cm}^{-1}$). The absorption minimum between $S_0 - S_1$ absorption and $S_0 - S_2$ absorption around 430 nm is better resolved in the ethyl acetate solution than in the polymer samples. Below 350 nm the absorption cross-section spectrum of the polymer samples could not be measured because of the polymer substrate absorption. For COPH(MMA-TMSPMA) in Fig. 4c the high absorption cross-sections below 440 nm seem to be a substrate artefact (no blank was available for substrate subtraction).

In Fig. 4 the stimulated emission cross-section spectra are also included. They are calculated from the $S_0 - S_1$ absorption cross-section spectra, $\sigma_a(\lambda)$, and the fluorescence quantum distributions, $E_F(\lambda)$, according to the Einstein relation [38, 39]

$$\sigma_{em}(\lambda) = \frac{\lambda^4 n_F}{n_A} \frac{E_F(\lambda)}{\int_{em} E_F(\lambda')\lambda'^3\,d\lambda'} \int_{abs} \frac{\sigma_a(\lambda')\,d\lambda'}{\lambda'}, \qquad (6)$$

where n_F is the mean refractive index in the fluorescence region, and n_A is the mean refractive index in the $S_0 - S_1$ absorption region. The $S_1 - S_0$ stimulated emission cross-section spectra ($\Delta\tilde{\nu}_{em} \approx 2700\,\mathrm{cm}^{-1}$ in ethyl acetate, and $\Delta\tilde{\nu}_{em} \approx 2400\,\mathrm{cm}^{-1}$ in polymer matrices) are broader than the $S_0 - S_1$ absorption cross-section spectra ($\Delta\tilde{\nu}_a \approx 1150\,\mathrm{cm}^{-1}$ in ethyl acetate, and $\Delta\tilde{\nu}_a \approx 1300\,\mathrm{cm}^{-1}$ in polymer matrices). For this reason the peak stimulated emission cross-sections are lower than the peak absorption cross-sections. The Stokes shift, $\delta\tilde{\nu}_{St}$, between the $S_0 - S_1$ absorption peak and emission peak is larger in ethyl acetate ($\delta\tilde{\nu}_{St} \approx 1940\,\mathrm{cm}^{-1}$) than in the polymer matrices ($\delta\tilde{\nu}_{St} \approx 1490\,\mathrm{cm}^{-1}$). Accordingly the stimulated emission cross-section spectra of the PM597 doped polymers are less red shifted than the stimulated emission cross-section spectrum of PM597 in ethyl acetate. The vibronic structure of the emission spectra of all PM597 samples is washed out. This smoothing indicates some inhomogeneous broadening of the emission spectra.

The fluorescence quantum distributions, $E_F(\lambda)$, are displayed in Fig. 5. The intrinsic fluorescence quantum yield, φ_F, is given by the integral of the fluorescence quantum distribution over the emission wavelength region, i.e. $\varphi_F = \int_{em} E_F(\lambda)\,d\lambda$. The determined fluorescence quantum yields are listed in Table 1. The fluorescence quantum yield of PM597 in ethyl acetate is $\varphi_F \approx 0.43$. In the polymer matrices the fluorescence quantum yield of PM597 is higher in the range of 60% to 70%. The non-radiative losses are reduced in the solid-state matrices probably due to reduction of internal conversion.

The determined degrees of fluorescence polarization, $P_F = (S_{F,||} - S_{F,\perp})/(S_{F,||} + S_{F,\perp})$, are listed in Table 1. In ethyl acetate the degree of fluorescence polarization is very small because of molecular reorientation within the fluorescence lifetime. The molecular reorientation time, τ_{or}, may be approximately determined by the Stokes–Einstein-relation [40, 41]

$$\tau_{or} = \frac{\eta V_h}{k_B \vartheta}, \qquad (7)$$

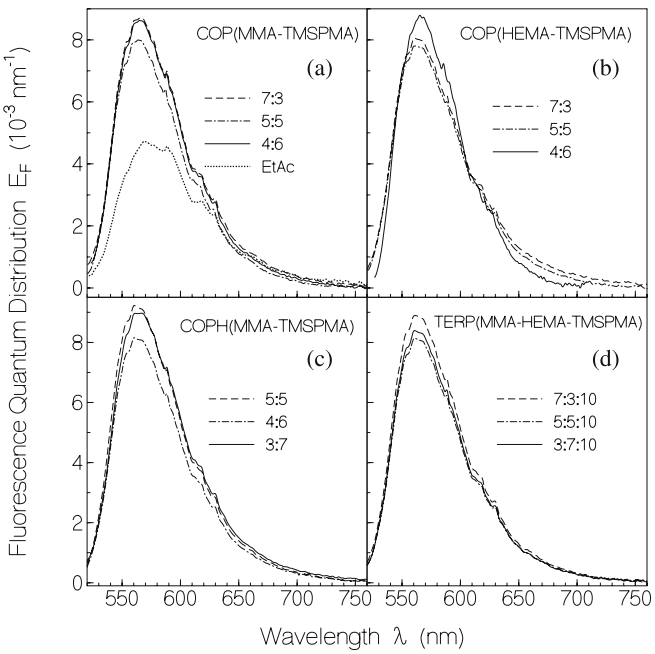

FIGURE 5 Fluorescence quantum distributions of PM597 doped polymer samples. Sample thickness 1 mm. PM597 concentrations are given in Table 1. In (**a**) the fluorescence quantum distribution of PM597 in solvent ethyl acetate is included

Parameter	Ethyl acetate	COP(MMA-TMSPMA)			COPH(MMA-TMSPMA)		
Volume ratio		7 : 3	5 : 5	4 : 6	5 : 5	4 : 6	3 : 7
C (mol dm^{-3})	9.2×10^{-6}	1.53×10^{-5}	1.33×10^{-5}	1.25×10^{-5}	1.94×10^{-5}	2.04×10^{-5}	2.27×10^{-5}
n_D	1.37216 [a]	1.4841	1.4810	1.4801	1.4870	1.4875	1.4865
$n_F - n_C$	0.00639	0.0098921	0.0092135	0.0089962	0.010897	0.010759	0.010889
φ_F	0.43	0.683	0.601	0.66	0.718	0.632	0.719
P_F	0.02±0.005	0.29±0.01	0.29±0.01	0.28±0.01	0.29±0.01	0.27±0.01	0.24±0.01
τ_{or} (ns)	0.14	7.2	7.0	6.6	7.7	6.5	5.2
τ_F (ns)	4.84	6.26±0.1	6.08±0.1	6.22±0.1	6.65±0.1	6.62±0.1	6.78±0.1
τ_{rad} (ns)	11.25	9.17	10.12	9.42	9.26	10.47	9.43
$\lambda_{a,p}$ (nm)	523	525	525	525	524.5	524.5	524.5
$\Delta\tilde{\nu}_a$ (cm^{-1})	1146	1310	1290	1290	1244	1244	1244
$\lambda_{em,p}$ (nm)	582	569	569	569	569	569	569
$\Delta\tilde{\nu}_a$ (cm^{-1})	2688	2456	2428	2428	2475	2313	2551
$\delta\tilde{\nu}_{St}$ (cm^{-1})	1938	1473	1473	1473	1491	1491	1491
$\sigma_{a,L}$ (10^{-16} cm^2)	2.09	1.765	1.82	1.85	1.74	1.79	1.8
$\sigma_{ex,L}$ (10^{-17} cm^2)	1±1	0.5±0.5			0.5±0.5		
$\varphi_{D,0}$	4×10^{-5} [b] 2.3×10^{-6} [c]	9×10^{-7}	1×10^{-6}	1.8×10^{-6}	2.5×10^{-6}	3×10^{-6}	7.3×10^{-6}
$\varphi_{D,\infty}$	4×10^{-5} [b] 7×10^{-6} [c]	1.1×10^{-7}	2×10^{-7}	2.2×10^{-7}	1.7×10^{-7}	1.6×10^{-7}	2×10^{-7}

Parameter	COP(HEMA-TMSPMA)			TERP(MMA-HEMA-TMSPMA)		
Volume ratio	7 : 3	5 : 5	4 : 6	7 : 3 : 10	5 : 5 : 10	3 : 7 : 10
C (mol dm^{-3})	1.06×10^{-5}	9.35×10^{-6}	9.64×10^{-6}	1.23×10^{-5}	1.15×10^{-5}	1.18×10^{-5}
n_D	1.4952	1.4957	1.4900	1.4880	1.4883	1.4840
$n_F - n_C$	0.0094252	0.0091335	0.0094026	0.0103895	0.0101848	0.0097843
φ_F	0.637	0.597	0.593	0.684	0.626	0.639
P_F	0.29±0.01	0.27±0.02	0.28±0.01	0.28±0.01	0.29±0.01	0.28±0.01
τ_{or} (ns)	6.5	6.0	6.3	6.4	6.9	6.7
τ_F (ns)	5.63±0.1	6.17±0.1	5.9±0.1	6.06±0.1	6.01±0.1	6.3±0.1
τ_{rad} (ns)	8.84	9.43	7.68	8.86	9.60	9.86
$\lambda_{a,p}$ (nm)	524.5	524.5	524.5	524.5	524.5	524.5
$\Delta\tilde{\nu}_a$ (cm^{-1})	1321	1277	1318	1288	1288	1288
$\lambda_{em,p}$ (nm)	569	569	569	569	569	569
$\Delta\tilde{\nu}_a$ (cm^{-1})	2484	2437	2451	2409	2423	2423
$\delta\tilde{\nu}_{St}$ (cm^{-1})	1491	1491	1491	1491	1491	1491
$\sigma_{a,L}$ (10^{-16} cm^2)	1.83	1.72	1.73	1.82	1.84	1.81
$\sigma_{ex,L}$ (10^{-17} cm^2)			0.5±0.5		0.5±0.5	
$\varphi_{D,0}$	2.2×10^{-5}	1×10^{-5}	6×10^{-6}	2×10^{-6}	2.6×10^{-6}	5.5×10^{-6}
$\varphi_{D,\infty}$	7.2×10^{-7}	$\approx 5 \times 10^{-7}$	3×10^{-7}	2×10^{-7}	7.8×10^{-7}	4.7×10^{-7}

[a] [52] 18.9 °C
[b] air-saturated
[c] de-aerated

TABLE 1 Parameters of PM597 doped polymers

where η is the dynamic viscosity, V_h is the hydrodynamic volume of the molecule, k_B is the Boltzmann constant, and ϑ is the temperature. We approximate the hydrodynamic volume, V_h, by twice the molecular volume, V_m, which is given by $V_m = M_m/(N_A\varrho)$, where M_m is the molar mass, N_A is the Avogadro constant, and ϱ is the mass density. Using $\eta = 4.55 \times 10^{-4}$ Pa s (1 Pa s = 10 Poise), $M_m = 374.32$ g mol^{-1}, $\varrho \approx 1$ g cm^{-3}, and $\vartheta = 293$ K, we estimate $\tau_{or} \approx 140$ ps for PM597 in ethyl acetate. The degree of fluorescence polarization, P_F, is related to the reorientation time, τ_{or}, of the transition dipole moment by the Perrin formula [42–44]

$$P_F = \frac{3P_0\tau_{or}}{3(\tau_{or}+\tau_F) - P_0\tau_F}, \tag{8}$$

where $P_0 = 0.5$ is the degree of fluorescence polarization in the absence of transition dipole reorientation ($\tau_{or} = \infty$). Using $\tau_{or} = 140$ ps gives $P_F = 0.017$ in reasonable agreement with the experimental finding of $P_F = 0.02 \pm 0.01$ for PM597 in ethyl acetate.

For PM597 immobilized in the polymer matrices a degree of fluorescence polarization of $P_F \approx 0.28$ was measured. This value corresponds to a reorientation time of the involved transition dipole moment in the absorption and emission process of $\tau_{or} \approx 6.6$ ns according to the relation [42–44]

$$\tau_{or} = \frac{1/P_0 - 1/3}{1 - P_F/P_0} P_F\tau_F. \tag{9}$$

The intensity dependent saturable absorption behaviour of PM597 in ethyl acetate and of PM597 in COP(MMA-TMSPMA 7 : 3) is shown in Fig. 6. The intrinsic dye transmissions measured versus ethyl acetate solvent or polymer blank are presented. Similar transmission bleaching curves were measured for PM597 in COPH(MMA-TMSPMA 5 : 5),

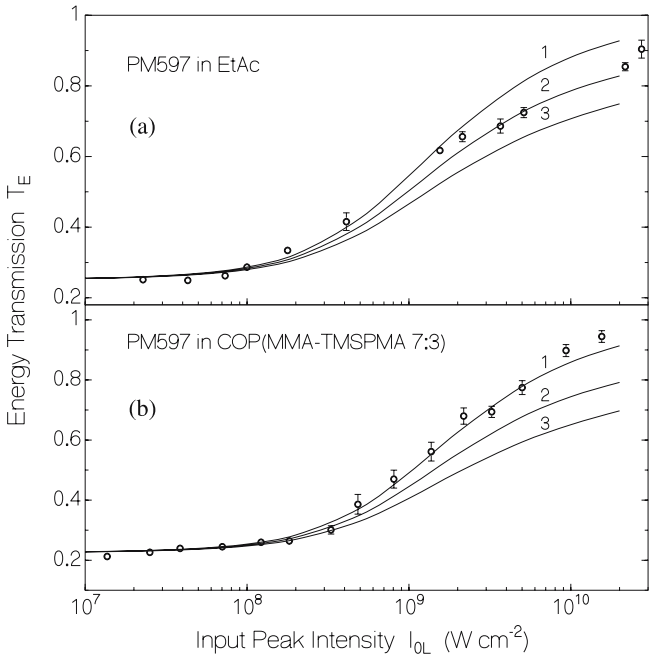

FIGURE 6 Intensity dependent energy transmission of (**a**) PM597 in ethyl acetate (cell length 1 mm), and (**b**) PM597 in COP(MMA-TMSPMA 7 : 3) (sample length 11 mm). *Circles* are experimental data. *Error bars* indicate the standard deviation of the mean values. The *curves* are calculated with parameters of Table 1 and (1) $\sigma_{ex,L} = 0$, (2) $\sigma_{ex,L} = 2 \times 10^{-17}$ cm^2, (3) $\sigma_{ex,L} = 4 \times 10^{-17}$ cm^2

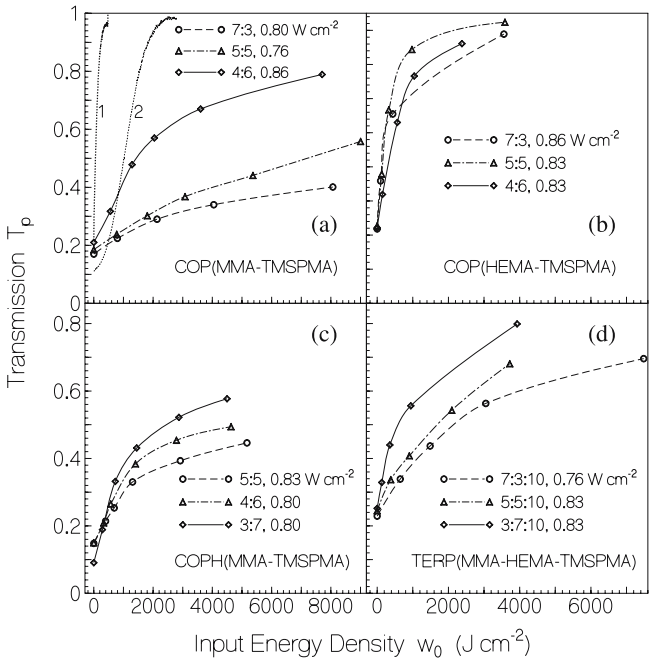

FIGURE 7 Photo-degradation of PM597. The transmission at peak $S_0 - S_1$ absorption wavelength, $\lambda_p = 525$ nm, versus exposed input energy density, w_0, at excitation wavelength $\lambda_{exc} = 514$ nm is shown. Excitation intensities are given in the legends. For PM597 in ethyl acetate, included in (**a**), the transmissions at $\lambda_{exc} = 514$ nm are given. There the excitation intensities are $I_{exc} = 0.21$ W cm^{-2} for an air-saturated solution (*curve* 1), and $I_{exc} = 0.36$ W cm^{-2} for a de-aerated solution (*curve* 2)

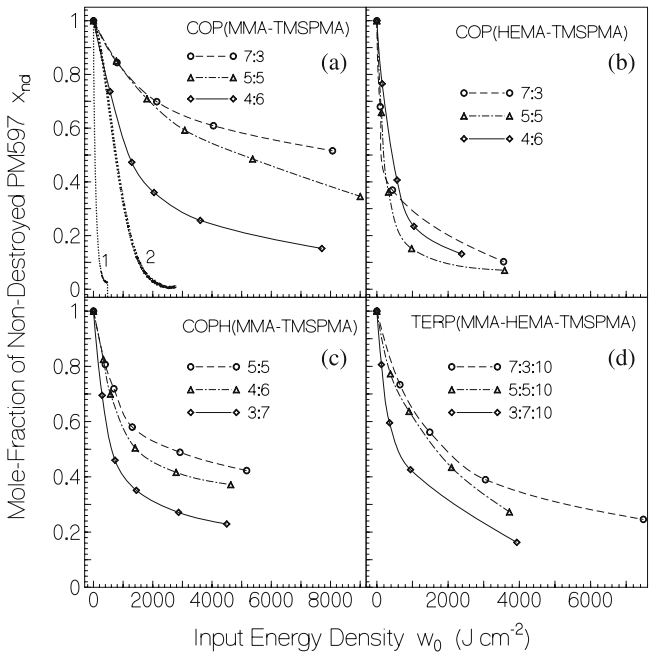

FIGURE 8 Fraction of non-destroyed PM597 molecules versus exposed input energy density, w_0, at excitation wavelength $\lambda_{exc} = 514$ nm. *Curves* are extracted from Fig. 7 by application of (10). As-delivered (1) and de-aerated (2) ethyl acetate solution results are included in (**a**)

COP(HEMA-TMSPMA 7 : 3), and TERP (MMA-HEMA-TMSPMA 7 : 3 : 10) (curves not shown). The intensity dependent energy transmission, $T_E(I_{0L})$, is determined by the small-signal transmission, T_0, the ground-state absorption cross-section, $\sigma_{a,L}$, at the pump laser wavelength, λ_L, and the excited-state absorption cross-section, $\sigma_{ex,L}$. The limiting transmission at high excitation intensity is caused by excited-state absorption. Since the limiting transmission approaches 100% the excited-state absorption at the pump laser wavelength is negligibly small.

The results of the photo-stability studies are presented in Fig. 7. The solid samples were excited at $\lambda_{exc} = 514$ nm with an intensity of $I_{exc} \approx 0.8$ W cm^{-2}, and the transmission was probed at $\lambda_p = 525$ nm. The measured transmission at the probe wavelength, λ_p, versus the exposed input excitation energy density, $w_0 = I_{exc} t_{exp}$, is plotted. The results of PM597 in air-saturated ethyl-acetate (as delivered) and in de-oxygenated ethyl-acetate (2 h of argon bubbling through the solution) are also included in Fig. 7a. In these cases the transmission of the excitation laser is shown ($\lambda_p = \lambda_{exc} = 514$ nm) whereby the excitation intensities were $I_{exc} = 0.21$ W cm^{-2} for the air-saturated sample and $I_{exc} = 0.36$ W cm^{-2} for the de-oxygenated sample.

The increase of transmission is due to PM597 photo-degradation. The recording of transmission spectra at certain times of exposure revealed a homogeneous decrease of absorption of the $S_0 - S_1$ absorption band (no new absorption band is formed for $\lambda > 440$ nm, which means that photoproducts start absorption at shorter wavelengths). After certain times of exposure fluorescence spectra were also recorded. The fluorescence spectra decreased in the same manner as the $S_0 - S_1$ absorption spectra. The shapes of the fluorescence spectra did not change with light exposure (curves not shown).

In Fig. 8 the mole-fraction of non-destroyed PM597 molecules, x_{nd}, versus exposed energy density is plotted. The curves are obtained by redrawing of Fig. 7. The mole-fraction

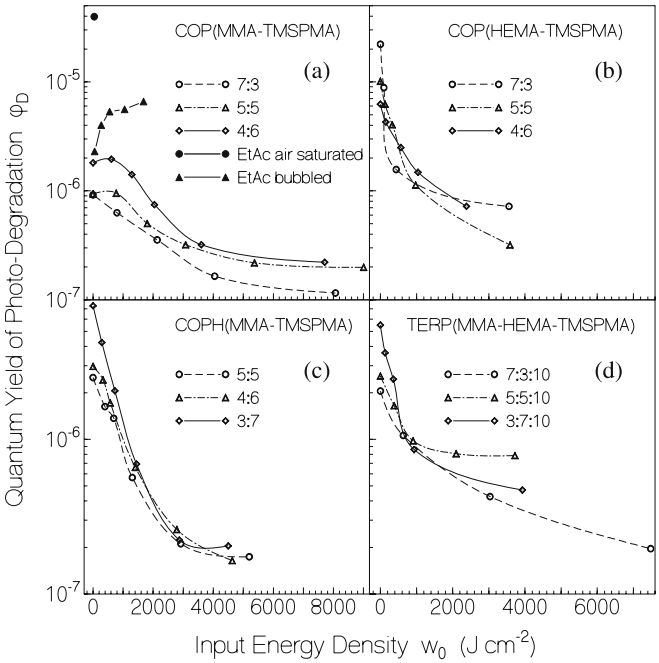

FIGURE 9 Dependence of quantum yield of photo-degradation, φ_D, on input energy density, w_0, for PM597 doped in polymers and for PM597 in ethyl acetate. The *curves* are calculated from results in Fig. 7 by use of (3)–(5)

of non-destroyed PM597 molecules is determined by the ratio of the absorbance, $A_p(w_0)$, of the samples at λ_p after light exposure with energy density w_0 to the initial absorbance, $A_p(0)$, before light exposure, i.e.

$$x_{nd} = \frac{A_p(w_0)}{A_p(0)} = \frac{-\log[T_p(w_0)]}{-\log[T_p(0)]} = \frac{N_{nd}}{N_0}\,. \tag{10}$$

The absorbance is given by $A_p = -\log(T_p) = \ln(10)\alpha_p\ell = \ln(10)N_{nd}\sigma_{a,p}\ell$. α_p is the absorption coefficient at the probe wavelength λ_p, ℓ is the sample length, and N_{nd} is the number density of non-destroyed PM597 molecules. $w_0 = I_{exc}t_{exp}$ is the exposed input excitation energy density. N_0 is the initial number density of PM597 molecules.

In Fig. 9 the quantum yield of photo-degradation as a function of exposed input energy density, w_0, is plotted. The curves are obtained from the curves in Fig. 7 by use of (3) to (5). The quantum yield of photo-degradation depends on the energy density already exposed to the sample, and it depends on the polymer matrix or the liquid solvent. For the polymer matrices the quantum yield of photo-degradation is highest (lowest photo-stability) at the beginning of exposure. With light exposure, the quantum yield of photo-degradation first decreases and then levels off to a constant value. Dissolved oxygen in the polymer samples is thought to be responsible for the initial enhanced photo-degradation.

4 Discussion

The doping of PM597 in the investigated silicon-containing organic polymer matrices has little influence on the $S_0 - S_1$ absorption spectrum: a spectral red-shift of about 1 nm and a slight spectral broadening compared to PM597 in ethyl acetate are observed.

The fluorescence spectra of PM597 in the solid matrices are about 10 nm less red-shifted than in the liquid sample. In both, the solid samples and the liquid sample, the fluorescence spectra are spectrally broader than the $S_0 - S_1$ absorption spectra leading to smaller stimulated $S_1 - S_0$ stimulated emission cross-sections compared to the corresponding $S_0 - S_1$ absorption cross-sections.

The fluorescence quantum yields of PM597 in the polymer matrices were found to be in the range of 60% to 70%, while in liquid ethyl acetate a fluorescence quantum yield of 43% was found. In [26] the fluorescence quantum yields of PM597 in a series of organic liquid solvents at room temperature were determined. They ranged from 35% in dimethylformamide to 49% in 2,2,2-trifluoroethanol. In the rigid polymer the non-radiative relaxation due to internal conversion seems to be reduced leading to a higher fluorescence quantum yield.

For PM597 immobilized in the polymer matrices the observed degree of fluorescence polarization, $P_F \approx 0.28$ is less than the expected value of $P_F = 0.5$ for a rigid molecule with an equal oriented absorption and emission transition dipole moment. It is expected that there occurs a charge-redistribution in the excited-state compared to the ground-state, changing the orientation of the transition dipole moment of emission relative to the transition dipole moment of absorption [26].

A reorientation of the excited molecules in the S_1 state by excitation energy transfer plays no role for our investigated samples of low dye concentration (1×10^{-5} to 2×10^{-5} mol dm^{-3}) as is shown by the following estimate. The quantum yield of Förster-type energy transfer, φ_{ET}, is approximately given by [45, 46]

$$\varphi_{ET} \approx \left(\frac{R_0}{R_d}\right)^6\,, \tag{11}$$

where R_0 is the critical Förster distance (there the energy transfer rate is equal to the excited state decay rate at infinitely low concentrations), R_d is the distance between the energy transfer partners (here the distance between two PM597 molecules). The critical Förster distance is given by [45–47]

$$R_0^6 = \frac{9\kappa^2}{128\pi^5 n^4}\int E_F(\lambda)\sigma_a(\lambda)\lambda^4\,d\lambda\,, \tag{12}$$

where $\kappa^2 = 2/3$ is an isotropic orientation factor, and n is the average refractive index of the sample in the overlap region of absorption and emission. Using our experimental parameters for PM597 in COP(MMA-TMSPMA 7 : 3) we find $R_0 = 3.9$ nm and $R_d \approx N_0^{-1/3} = 47.7$ nm ($N_0 = 9.2 \times 10^{15}$ cm^{-3}) giving $\varphi_{ET} \approx 3 \times 10^{-7}$. This small quantum yield shows that Förster type energy transfer plays no role for the investigated sample and does not contribute to the fluorescence depolarization.

The nonlinear transmission measurements displayed in Fig. 6 show nearly complete absorption bleaching at a high picosecond pump laser intensity indicating negligible excited-state absorption at the excitation laser wavelength. The solid curves in Fig. 6 are numerical simulations to the transmission measurements. The applied energy level system for the saturable absorption simulations is shown in Fig. 10. The

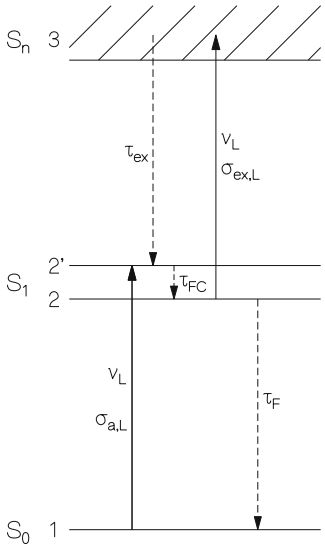

FIGURE 10 Energy level diagram used for saturable absorption simulations

pump laser excites chromophores from the S_0 ground-state 1 to a Franck–Condon level $2'$ in the S_1 band. From there the chromophores relax to a thermalized level 2 with the Franck–Condon relaxation time constant, τ_{FC} ($\tau_{FC} = 0.5$ ps is used in simulations [48]). From the S_1 band excited-state absorption occurs to a higher lying singlet band S_n (level 3). The higher excited chromophores relax quickly back to the S_1 band with a time constant, τ_{ex} ($\tau_{ex} = 60$ fs is used in simulations [49]).

The differential equation system for the intensity dependent pump pulse transmission is given in [50] [equations (6)–(14)] and is not repeated here. The curves in Fig. 6 are calculated with the parameters given in Table 1 and in the caption of Fig. 6. The excited-state absorption cross-section, $\sigma_{ex,L}$, is varied. The obtained $\sigma_{ex,L}$ values are listed in Table 1. They are close to $\sigma_{ex,L} = 0$ indicating negligible excited-state absorption.

The studies of the photo-stability of PM597 in ethyl acetate and in the different silicon-containing polymers showed an enormous stability improvement in the solid samples and a stability optimization by polymer composition.

The degree of photo-degradation is highest for PM597 in as-delivered ethyl acetate, where $\varphi_D \approx 4 \times 10^{-5}$ was determined (on the average damage after $\varphi_D^{-1} \approx 25\,000$ excitation cycles). For PM597 in de-aerated ethyl acetate solution the initial quantum yield of photo-degradation was found to be $\varphi_D \approx 2.3 \times 10^{-6}$, and it increased to about $\varphi_D \approx 6 \times 10^{-6}$ after some time of exposure. Photoproducts or photoproduct intermediates (likely radicals) seem to enhance the photo-degradation [6, 27, 51].

Figure 9 shows the quantum yield of photo-degradation of the remaining non-destroyed molecules after the samples were exposed to an input energy density of w_0, and Fig. 8 shows the mole-fraction of non-destroyed molecules after an exposure energy density of w_0 on the samples. After a long-time exposure the lowest quantum yield of photo-degradation of $\varphi_D \approx 1.2 \times 10^{-7}$ (highest photo-stability) and the highest mole-fraction of non-destroyed molecules of $x_{nd} \approx 0.52$ was found for PM597 in COP(MMA-TMSPMA 7 : 3). The PM597/COPH(MMA-TMSPMA) samples are nearly as photo-stable as the PM597/COP(MMA-TMSPMA) samples. Under the investigated solid-state samples the PM597/COP (HEMA-TMSPMA) samples have the lowest photo-stability. Generally the polymers with higher MMA content exhibit a higher photo-stability. The photo-stability of PM597 in de-aerated ethyl acetate is considerably less than the photo-stability of PM597 in all the investigated solid matrices, and PM597 in as-delivered ethyl acetate is considerably less photo-stable than in de-aerated ethyl acetate.

The laser performance of PM597 in COP(MMA-TMSPMA), COP(HEMA-TMSPMA), and COP(MMA-HEMA-TMSPMA) was studied in [22]. Pumping the samples with 6 ns second harmonic pulses of a Q-switched Nd:YAG laser (single pulse energy 5.5 mJ) at 10 Hz repetition rate caused no reduction of laser performance (no reduction of dye laser output energy) within 100 000 laser shots at the same excitation spot. A similar behaviour was found for COPH(MMA-TMSPMA) (unpublished results). The reported laser performance data are in agreement with the photo-degradation results reported here, where for all polymer samples, a long-time-exposure photo-stability of $> 10^6$ photo-excitation cycles was determined.

5 Conclusions

The investigated samples of PM597 in silicon-containing organic matrices revealed good photo-physical properties for solid-state dye laser action. The fluorescence quantum yield was found to be in the 60% to 70% region, and was not strongly influenced by the copolymer and terpolymer composition. For all investigated polymer compositions the quantum yield of photo-degradation was found to be less than 10^{-6} after some initial fading. The photo-stability turned out to be dependent on the specific copolymer and terpolymer class and the component mixing ratio. For the best sample of PM597/COP(MMA-TMSPMA 7 : 3) a final-state quantum yield of photo-degradation of $\varphi_D \approx 1.2 \times 10^{-7}$ was obtained corresponding on average to 8×10^6 excitation cycles before degradation. The determined high photo-stability agrees with laser performance studies [22] where the laser output after 100 000 shots with Q-switched laser pumping of the same excitation spot was just as high as it was at the beginning.

ACKNOWLEDGEMENTS The authors thank Mrs. Anja Merkel for skilful mechanical assistance. This work was partially supported by Poject N° MAT2004-04643-C03-01 of Spanish CICYT. D.d.A. thanks the Comunidad Autónoma de Madrid (CAM) for a predoctoral scholarship.

REFERENCES

1 A. Costela, I. García-Moreno, R. Sastre, In: *Handbook of Advanced Electronic and Photonic Materials and Devices*, ed. by H.S. Nalwa, (Academic Press, San Diego, CA, 2001) Vol. 7, p. 161
2 T.G. Pavlopoulos, J.H. Boyer, K. Thanggaraj, G. Sathyamoorthi, M.P. Shah, M.L. Soong, Appl. Opt. **31**, 7089 (1992)
3 T.G. Pavlopoulos, Prog. Quantum Electron. **26**, 193 (2002)
4 A. Costela, I. García-Moreno, R. Sastre, Phys. Chem. Chem. Phys. **5**, 4745 (2003)
5 A. Costela, I. García-Moreno, C. Gómez, O. García, R. Sastre, Chem. Phys. Lett. **369**, 656 (2003)
6 M. Ahmad, T.A. King, D. Ko, B.H. Cha, J. Lee, Opt. Commun. **203**, 327 (2002)

7 Q.Y. Zhang, W.X. Que, S. Buddhudu, K. Pita, J. Phys. Chem. Solids **63**, 1723 (2002)
8 T.H. Nhung, M. Canva, T.T.A. Dao, F. Chaput, A. Brun, N.D. Hung, J.P. Boilot, Appl. Opt. **42**, 2213 (2003)
9 Y. Yang, M. Wang, G. Qian, Z. Wang, X. Fan, Opt. Mater. **24**, 621 (2004)
10 F. Amat-Guerri, M. Carrascoso, M. Liras, R. Sastre, Photochem. Photobiol. **77**, 577 (2003)
11 F. López Arbeloa, J. Bañuelos Prieto, I. López Arbeloa, A. Costela, I. García-Moreno, C. Gómez, F. Amat-Guerri, M. Liras, R. Sastre, Photochem. Photobiol. **78**, 30 (2003)
12 A. Bergmann, W. Holzer, R. Stark, H. Gratz, A. Penzkofer, F. Amat-Guerri, A. Costela, I. García-Moreno, R. Sastre, Chem. Phys. **271**, 201 (2001)
13 I. García-Moreno, A. Costela, L. Campo, R. Sastre, F. Amat-Guerri, M. Liras, F. López Arbeloa, J. Bañuelos Prieto, I. López Arbeloa, J. Phys. Chem. A **108**, 3315 (2004)
14 A. Costela, I. García-Moreno, C. Gómez, F. Amat-Guerri, M. Liras, R. Sastre, Appl. Phys. B **76**, 365 (2003)
15 M. Álvarez, F. Amat-Guerri, A. Costela, I. García-Moreno, C. Gómez, M. Liras, R. Sastre, Appl. Phys. B **80**, 993 (2005)
16 A.J. Finlayson, N. Peters, P.V. Kolinsky, M.R.W. Venner, Appl. Phys. Lett. **75**, 457 (1999)
17 V.S. Nechitailo, R.S. Anderson, S.C. Picarello, G.A. Matyushin, J.H. Bohn, Proc. SPIE **3613**, 106 (1999)
18 X. Xudong, H. Lili, H. Guosong, J. Zhonghong, Chin. J. Lasers A **27**, 307 (2000)
19 H.R. Aldag, S.M. Dolotov, M.F. Koldunov, Ya.V. Krachenko, A.A. Malenkov, D.P. Pacheco, A.V. Reznichenko, G.P. Roskova, Proc. SPIE **3929**, 133 (2000)
20 E. Yariv, S. Schultheiss, T. Saradarov, R. Reisfeld, Opt. Mater. **16**, 29 (2001)
21 S.Y. Lam, M.J. Damzen, Appl. Phys B **77**, 577 (2003)
22 A. Costela, I. García-Moreno, D. del Agua, O. García, R. Sastre, Appl. Phys. Lett. **85**, 2160 (2004)
23 R. Jakubiak, L.V. Natarajan, V. Tondiglia, G. He, P.N. Prasad, T.J. Bunning, R.A. Vaia, Appl. Phys. Lett. **85**, 6095 (2004)
24 H.C. Lee, Y.P. Kim, Hankook Kwanghak Hoeji **16**, 143 (2005)
25 G.S. He, P.N. Prasad, IEEE J. Quantum Electron. **QE-34**, 473 (1998)
26 J.B. Prieto, F.L. Arbeloa, V.M. Martínez, T.A. López, I.L. Arbeloa, J. Phys. Chem. A **108**, 5503 (2004)
27 N. Tanaka, W.N. Sisk, J. Photochem. Photobiol. A **172**, 109 (2005)
28 R. Reisfeld, E. Yariv, H. Minti, Opt. Mater. **8**, 31 (1997)
29 I. García-Moreno, A. Costela, A. Cuesta, O. García, D. del Agua, R. Sastre, J. Phys. Chem. B. **109**, 21618 (2005)
30 L.W. Tilton, J.K. Taylor, In: *Physical methods in Chemical Analysis*, ed. by W.G. Berl, (Academic Press, New York, 1960) Vol. 1
31 A. Penzkofer, H. Glas, J. Schmailzl, Chem. Phys. **70**, 47 (1982)
32 A. Penzkofer, W. Leupacher, J. Luminesc. **37**, 61 (1987)
33 W. Holzer, M. Pichlmaier, A. Penzkofer, D.D.C. Bradley, W.J. Blau, Chem. Phys. **246**, 445 (1999)
34 W. Bäumler, A. Penzkofer, Chem. Phys. **140**, 75 (1990)
35 F. Dörr, Angew. Chem. **78**, 457 (1966)
36 A. Penzkofer, Appl. Phys. B **46**, 43 (1988)
37 W. Scheidler, A. Penzkofer, Opt. Commun. **80**, 127 (1990)
38 O.G. Peterson, J.P. Webb, W.C. McColgin, J.H. Eberly, J. Appl. Phys. **42**, 1917 (1971)
39 A.V. Deshpande, A. Beidoun, A. Penzkofer, G. Wagenblast, Chem. Phys. **142**, 123 (1990)
40 T.J. Chuang, K.B. Eisenthal, Chem. Phys. Lett. **11**, 368 (1971)
41 H.E. Lessing, A. von Jena, In: *Laser Handbook*, ed. by M.L. Stitch, (North-Holland, Amsterdam, 1979) Vol. 3, pp.753
42 C.A. Parker, *Photoluminescence of Solutions* (Elsevier, Amsterdam, 1968)
43 G. Weber, In: *Fluorescence and Phosphorescence Analysis, Principles and Applications*, ed. by D.M. Hercules, (Interscience, New York, 1966), p. 217
44 P. Weidner, A. Penzkofer, Chem. Phys. **191**, 303 (1995)
45 T. Förster, *Fluoreszenz organischer Verbindungen* (Vandenhoeck und Ruprecht, Göttingen, 1951)
46 G.R. Fleming, *Chemical Applications of Ultrafast Spectroscopy* (Oxford University Press, New York, 1986)
47 F. Ammer, A. Penzkofer, P. Weidner, Chem. Phys. **192**, 325 (1995)
48 A. Penzkofer, W. Falkenstein, W. Kaiser, Chem. Phys. Lett. **44**, 82 (1976)
49 F. Graf, A. Penzkofer, Opt. Quantum Electron. **17**, 53 (1989)
50 W. Holzer, H. Gratz, T. Schmitt, A. Penzkofer, A. Costela, I. García-Moreno, R. Sastre, F.J. Duarte, Chem. Phys. **256**, 125 (2000)
51 K.-S. Kang, W.N. Sisk, M.Y.A. Raja, F. Farahi, J. Photochem. Photobiol. A **121**, 133 (1999)
52 E.W. Washburn (ed.), *International Critical Tables of Numerical Data, Physics, Chemistry and Technology* (McGraw Hill, New York, 1930) Vol. VII, p. 36